Concrete Beton, Volume 123, pp 8-15, November 2009

Constitutive Model for Fibre-reinforced Strain-hardening Cement Composites (SHCC)

AUTHOR: G P A G van Zijl

Department of Civil Engineering, Stellenbosch University, South Africa

ABSTRACT: Constitutive models that capture dominating mechanisms of mechanical and time-dependent behaviour of construction materials, are essential for accurate structural analysis. Such models may be highly complex, as the behaviour of, especially cement-based construction materials, is indeed complex. The value of such models lies in the ability it affords the specialist to predict structural behaviour beyond that measured in physical experiments, which is a cost-effective extension of the physical experiment data. With the aid of such complex models, thorough understanding and eventual simpler analytical models can be derived. This paper describes a constitutive model for fibre-reinforced strain-hardening cement composites (SHCC).

Journal Contact Details:
PO Box 75364
Lynnwood Ridge
Pretoria, 0040
South Africa
+27 12 348 5305

admin@concretesociety.co.za
www.concretesociety.co.za

CONCRETE SOCIETY
OF SOUTHERN AFRICA

Constitutive model for fibre-reinforced strain-hardening cement composites (SHCC)

By GPAG van Zijl
Department of Civil Engineering, Stellenbosch University, South Africa

ABSTRACT: Constitutive models that capture dominating mechanisms of mechanical and time-dependent behaviour of construction materials are essential for accurate structural analysis. Such models may be highly complex, as the behaviour of especially cement-based construction materials is indeed complex. The value of such models lies in the ability it affords the specialist to predict structural behaviour beyond that measured in physical experiments, which is a cost-effective extension of the physical experimental data.
With the aid of such complex models, thorough understanding and eventual simpler analytical models can be derived. This paper describes a constitutive model for fibre-reinforced strain-hardening cement composites (SHCC).


GPAG van Zijl

SHCC is a relatively new class of high performance fibre-reinforced cement-based composites (HPFRCC), which currently receives intensive research attention internationally. Physical evidence of rate and time-dependence of SHCC is presented in terms of tensile rate-dependent test results, as well as tensile creep test results. A model for time-dependent mechanical behaviour of SHCC is proposed and elaborated. The model is based in multi-surface, anisotropic, computational continuum plasticity. It is shown to realistically capture rate-enhanced tensile resistance, as well as tensile creep fracture.

1 INTRODUCTION

This paper proposes a constitutive model for fibre re-inforced strain-hardening cement composites (SHCC). This class of high performance fibre reinforced cement composite (HPFRCC) is designed for large tensile strain capacity at moderate tensile strength, with examples shown in *Figure 1*. A high tensile strength FRCC is also shown in the figure.

The tensile ductility of SHCC is obtained through balanced fibre and matrix properties, to allow effective crack bridging by fibres, whereby cracks are controlled to widths in the micro-range, despite moderate fibre volume levels ($1.5<V_f<2.5\%$). Evidence is emerging that the crack control is maintained also in more general loading conditions, including flexure, shear (Shang & van Zijl 2007) and combined flexure and shear, both in pure SHCC and with steel bar reinforcement (R/SHCC) (van Zijl 2008).

The significance of the crack control is reduced water and chloride diffusivity through crack width limitation in cement composites, as reported by several researchers (Wang *et al.* 1997, Rapoport

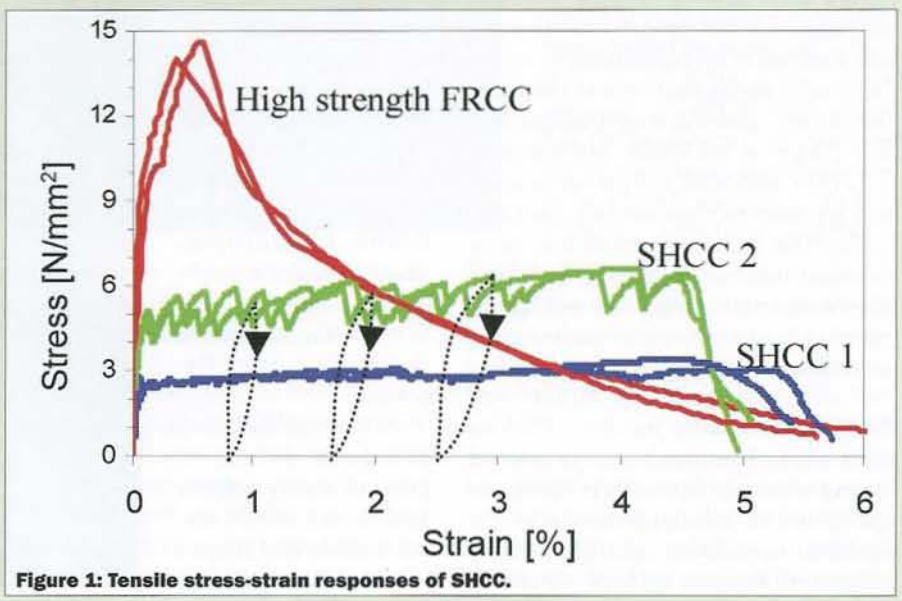

Figure 1: Tensile stress-strain responses of SHCC.

Ingredient	Mass proportion	kg/m³
Cement (CEM I 42.5)	0.5	531
Fly Ash	0.5	531
Water	0.4	425
Sand (φ_s<0.21 mm)	0.5	531
PVA fibre, L_f = 12 mm, d_f = 0.04 mm	0.024	26

Table 1: Typical SHCC mix proportions

et al. 2001, Lepech & Li 2005, Sahmaran *et al.* 2007).

These processes govern the longer term migration of water and chlorides into the material through the micropores (Bažant, & Najjar 1971, Neithalath 2006).

Under service conditions, which inevitably include cracks in cement composites, long term durability is controlled by reduced diffusivity. The experimental evidence that crack widths may be limited to within a threshold value of 100μm by inherent crack control in SHCC (Weimann & Li 2003) confirms the potential of SHCC for durable structures.

To enable sound application of SHCC, design models are required, which should eventually be incorporated in standards for structural design with this construction material. Such models do not yet exist, and the pool of experimental data is limited relative to traditional construction materials like reinforced concrete and structural steel. It is argued that computational models, in combination with physical experiments, are effective in developing insight in the behaviour of structures manufactured of such a new material, thereby assisting in the formulation of simpler design models. Such computational models should capture the main mechanisms of behaviour with reasonable accuracy to be objective and allow prediction of structural behaviour beyond that tested in physical experiments.

While detailed micro-models may prove more accurate by capturing interaction of the heterogeneities in SHCC (fibres, hcp matrix, fibre-matrix interfaces), so-called macro-models are pragmatic and allow viable analysis and prediction of structural behaviour.

In this paper a macro-model based on continuum plasticity is proposed and elaborated. Such a model does not distinguish between the various ingredients in SHCC, but considers it to be a homogeneous continuum.

The use of such continuum models for concrete or other cement-based material have become standard in research environments and are even available in commercial finite element packages such as DIANA (2008), which is used in this research.

However, a computational macro-model appropriate for SHCC does not yet exist commercially. A model based on continuum damage was proposed recently by Boshoff & van Zijl (2007), but provided for non-linear behaviour in only the tensile regime.

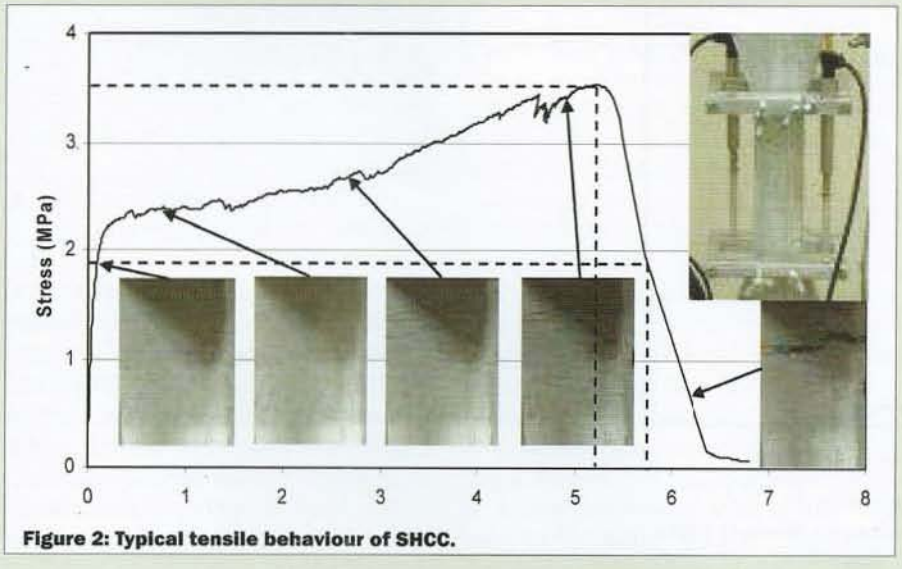

Figure 2: Typical tensile behaviour of SHCC.

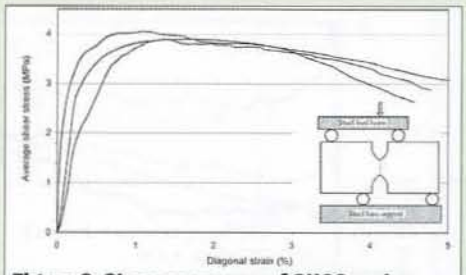

Figure 3: Shear response of SHCC under pure shear (Shang &van Zijl 2007).

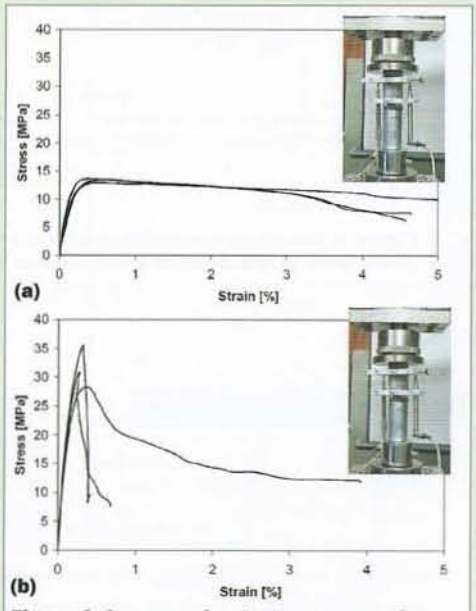

Figure 4: Compression test response of SHCC cylinder specimen 100 mm x 50 mm diameter produced by (a) casting (W/B = 0.4) and (b) extrusion (W/B = 0.25)

Also, reported SHCC response to cyclic loading (Boshoff 2007, Jun & Mechtcherine 2007) indicates that elastic unloading, as used in a plasticity approach, is more appropriate for SHCC than the secant unloading used in the damage approach. Typical unloading-reloading behaviour is shown schematically in *Figure 1*.

Kabele (2002) also proposed a continuum model for SHCC. This model is limited to tensile non-linearity, and static behaviour, ie time-dependence is not incorporated. The unloading behaviour is elastic in the strain-hardening tensile regime, but secant beyond the peak tensile resistance.

In this paper, a continuum model is proposed for both tensile and compressive behaviour, in terms of a multi-surface continuum plasticity model. Anisotropy is considered in terms of different strengths and hardening-softening responses in orthogonal directions. This has been shown to be relevant for certain manufacturing processes, for instance extrusion, which predominantly

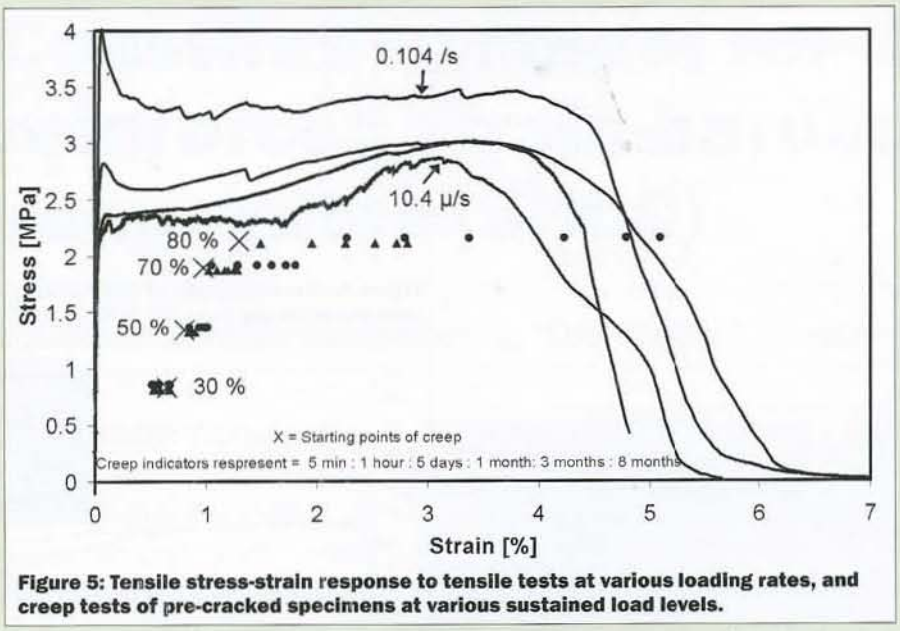

Figure 5: Tensile stress-strain response to tensile tests at various loading rates, and creep tests of pre-cracked specimens at various sustained load levels.

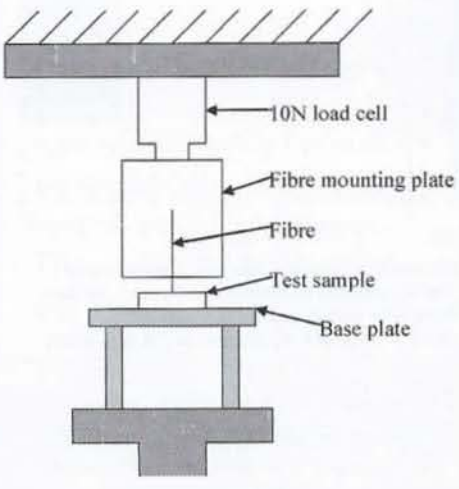

Figure 6

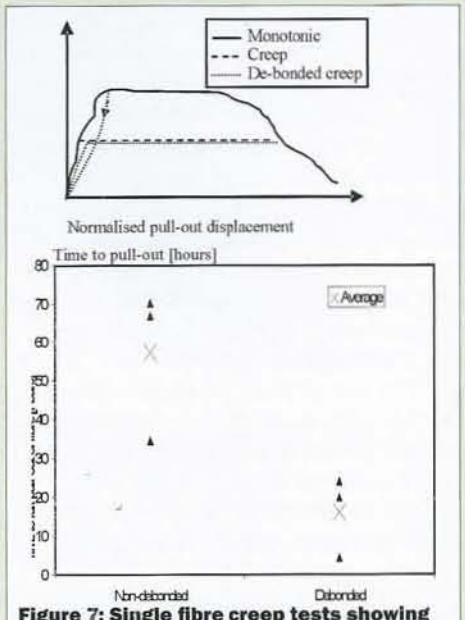

Figure 7: Single fibre creep tests showing (left) the load-deformation and (right) the times to failure (Boshoff 2007).

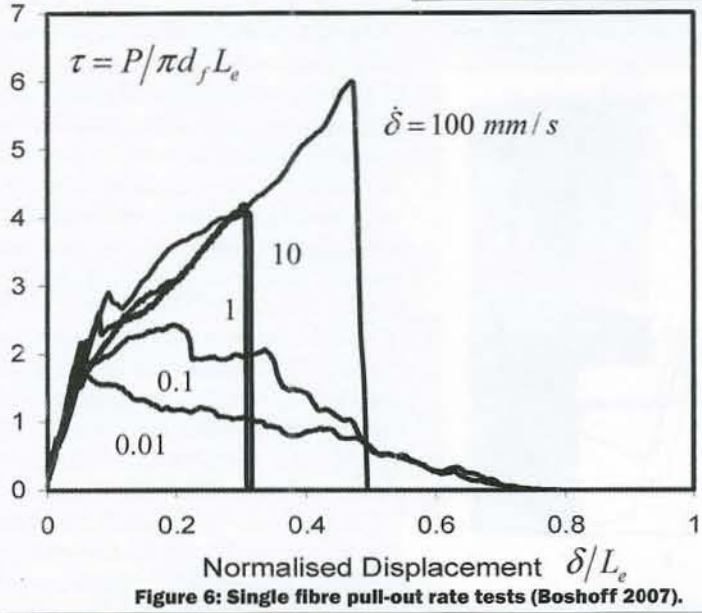

Figure 6: Single fibre pull-out rate tests (Boshoff 2007).

orientates fibres in the extrusion direction. Creep is incorporated in the form of visco-elasticity. In tension, cracking rate-dependence is considered, based on experimental evidence.

2 MECHANICAL BEHAVIOUR OF SHCC

Typical SHCC mechanical behaviour is demonstrated here by results of characterisation tests on a particular SHCC with mix proportions given in *Table 1*, used for all results reported in this paper, unless stated otherwise.

The specimens were produced by normal casting in steel moulds, stripping after two days and curing to an age of 14 days in water at controlled temperature of 23 °C. The evolutions of mechanical properties (7 days to 28 days, wet curing) have been reported before (van Zijl 2005). The tensile results here are for thin dumbbell specimens, shown in *Figure 2*, with typical thickness of 15 mm. Compressive results are however for 50 mm diameter cylinders of height 100 mm.

The strain-hardening response of SHCC is associated with multiple crack formation once the tensile strength of the matrix is exceeded. This is shown for a typical case in *Figure 2*.

Instead of significant widening of the first crack, which initiates once the matrix strength is exceeded, more cracks arise upon further deformation. The crack control is a dominant feature of SHCC and holds the key to understanding and predicting its short and long term behaviour.

Through balanced properties of the cement matrix, fibres and their interfaces, based on consideration of micro-mechanical mechanisms (Li *et al.* 1995), pseudo strain-hardening tensile behaviour is achieved.

The conditions for pseudo strain-hardening are well understood and the data base of experimental results towards confirming micromechanical design models is growing.

The ductility of SHCC is shown to exist also under pure shear (*Figure 3*) and uniaxial compression (*Figure 4a*).

Note that the SHCC produced by extrusion (*Figure 4b*) has significantly higher uniaxial compressive strength, due to the lower W/B ratio used to obtain extrudable SHCC, but also due to the high pressure extrusion process and fibre alignment in the extrusion direction.

This high strength is seen to be followed by a steep post-peak reduction in

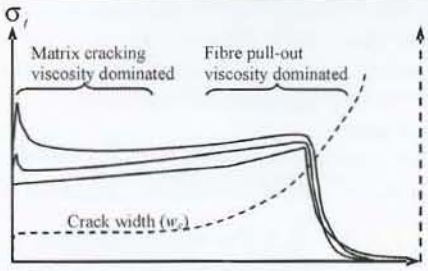

Figure 8: Trends in macroscopic tensile behaviour and mechanisms of rate-dependence.

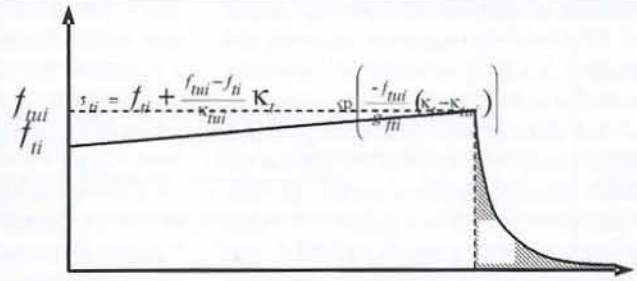

Figure 9: Tensile material law for SHCC.

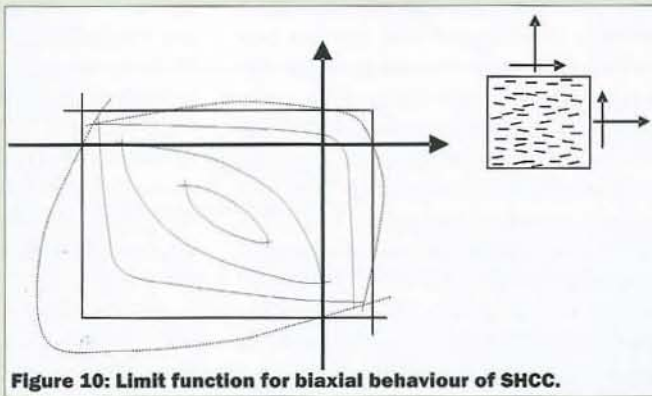

Figure 10: Limit function for biaxial behaviour of SHCC.

compressive resistance. The responses of cast SHCC suggest the use of ductile strain-hardening-softening relations to describe the stress-strain responses.

3 TIME DEPENDENT BEHAVIOUR OF SHCC

To illustrate the time dependent behaviour of SHCC under mechanical load, results of recent characterizing creep and rate-dependent tensile tests are summarised here. Tests were performed on macro-level as well as on single fibre pull-out level. For the macro tests, the same dumbbell-shaped specimens as in the previous section were prepared and tested. In addition, single fibre pull-out tests were performed. These specimens were prepared with the same matrix, but with a single fibre embedded to a pre-determined embedment length L_e. A series of tests were performed on specimens with different embedment lengths to establish a length suitable for subsequent test series at various pull-out rates, as well as under sustained load. From the initial test series L_e = 1.4 mm was chosen for the rate and creep tests. See Boshoff (2007) for complete details.

3.1 Rate dependence

3.1.1 Rate-dependent response of SHCC composite

Stress-strain responses of a series of tensile rate tests over 4 orders of average strain rate magnitudes ($10^{-5} \le \dot{\varepsilon} \le 10^{-1} s^{-1}$) are shown by the solid lines in *Figure 5*. The first cracking strength appears to be significantly rate-dependent, but the ultimate tensile strength and strain to a lesser degree.

3.1.2 Single fibre pull-out rate dependence

To study the rate effect on the micro-level, single fibre pull-out tests were performed (Boshoff 2007) at pull-out displacement rates over 4 orders of magnitude ($10^{-2} \le \dot{\delta} \le 10^{2}$ *mm/s*). Typical results are shown in *Figure 6*. A significant increase in peak pull-out force is seen with increased loading rate. At low rates, fibres pull out of the matrix completely, indicated by the gradual reduced resistance beyond the peak in *Figure 6*. Higher rates lead to fibre breakage, followed by an abrupt drop in resistance.

Thus it appears that fibre pull-out rate-dependence is an important mechanism of rate-dependence of the composite material.

3.2 Tensile creep response

The reduced stiffness and resistance of cement-based composites under long term sustained load are well described in the literature (eg. Rüsch 1960, Zhou 1992). This has recently been studied for SHCC in tension by Boshoff (2007). Two series of tests were performed.

3.2.1 Macro creep

Firstly, creep tests of previously undamaged specimens were performed at 50% of the ultimate tensile strength. Secondly, a series of creep tests was performed at various load levels (30%, 50%, 70% and 80% of average peak strength). Note that all the specimens of the second series were pre-cracked by deformation controlled tensile loading to a predetermined tensile strain of 1%. After this preload the specimens were unloaded and subsequently reloaded to the creep load, sustained for a period of eight months. The specimens were kept in a constant environment of 23±1 °C and 65%±5% RH. Two specimens were tested at each load level. The creep strain of the uncracked creep specimens at 50% of peak strength was in the order of 0.15% after 8 months. This is negligible relative to that of the pre-cracked specimens shown in *Figure 5*.

Note that the reduced stiffness is due to the pre-cracking.

After eight months no specimens failed, despite the quasi-static load-deformation/stress-strain envelope being exceeded in the case of the highest (80%) sustained load. Due to the sealant, cracks and spacing could not be observed or measured accurately.

However, individual cracks which existed at the onset of sustained loading were observed to widen in time. Instantaneous jumps in the time dependent deformation graphs provide evidence of new cracks initiating under the sustained load (Boshoff 2007). Both these two sources of time-dependent deformation were confirmed by creep tests performed by Jun & Mechtcherine (2007) and Boshoff *et al.* (2008).

3.2.2 Single fibre pull-out creep

Single fibre pull-out creep tests were also performed to study this important mechanism of creep in the composite. A sustained load causing a bond stress between the fibre and the matrix equalling τ = 1.2 *MPa* was applied, reached by an initial pull-out rate of 1 mm/s. Note that this represents an average normal fibre stress of roughly 1.6 times the average fibre stress in the composite at 80% of

the peak load (composite average stress 2.1 MPa). If a correction is made for the random 2D fibre orientation, whereby fewer fibres effectively bridge the crack, but at higher stress, the single fibre sustained load is representative of the composite situation. In a first series the fibre in each specimen was initially de-bonded by loading the fibre to just beyond τ_0 and then unloading, before commencing with the creep test. τ_0 is the average bond stress which marks the end of the linear load pull-out response. In a second series of three specimens, the test was performed on the undamaged (non de-bonded) specimen. In *Figure 7* the creep tests and resulting times to complete pull-out, or failure, are shown.

To distinguish fibre creep from the pull-out creep deformation, the time-dependent deformation of a single fibre was measured under a sustained normal stress of 580 MPa. This creep load is nearly five times the fibre normal stress in the pull-out creep stress.

Under these conditions insignificant time-dependent deformation of the fibre was measured. Thus, time dependent fibre pull-out appears to be an important mechanism of creep in the composite material.

3.2.3 Creep mechanisms

From the previous sections the main mechanisms of creep are identified as (i) the initiation of new cracks under sustained load, (ii) widening of cracks due to fibre pull-out, (iii) matrix creep. It was shown for the particular fibre that a potential fourth mechanism, namely fibre creep, does not contribute to creep in the SHCC studied here. It was also noted in section 3.2.1 that the uncracked matrix creep is small relative to the time-dependent deformation of cracked specimens, which implies that the mechanisms of crack initiation and widening due to fibre pull-out dominate.

To interpret these creep mechanisms, it is useful to study the trends in macroscopic tensile behaviour (*Figure 5*), in close connection with the micro behaviour of individual fibre pull-out (*Figures 6 and 7*), as well as micro-crack formation. The result of such scrutiny is presented as a schematised postulation in Figure 8. Also shown in this schematic figure as a dashed line is the crack width development, based on results reported by Boshoff *et al.* 2008. Cracks are controlled to small widths (in the range 50-150μm) over a large tensile deformation range. Such small crack widths imply that the lengths of fibres pulled out at the positions of cracks are also this small. This means that fibre pull-out cannot be the mechanism in the early strain-hardening stages, because the rate-enhanced resistance is mobilised at larger pull-out lengths, apparent from *Figure 6*. Only once the crack width increases, ie towards the end of the strain-hardening regime in *Figure 8*, this mechanism is activated.

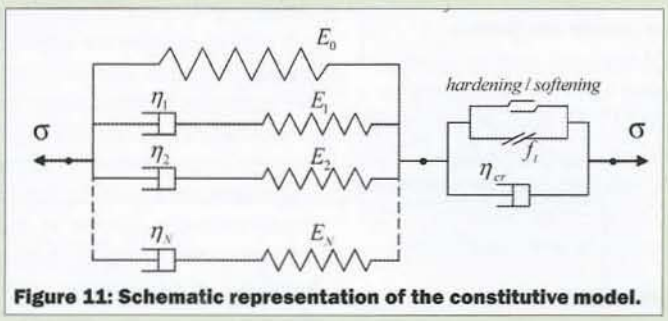

Figure 11: Schematic representation of the constitutive model.

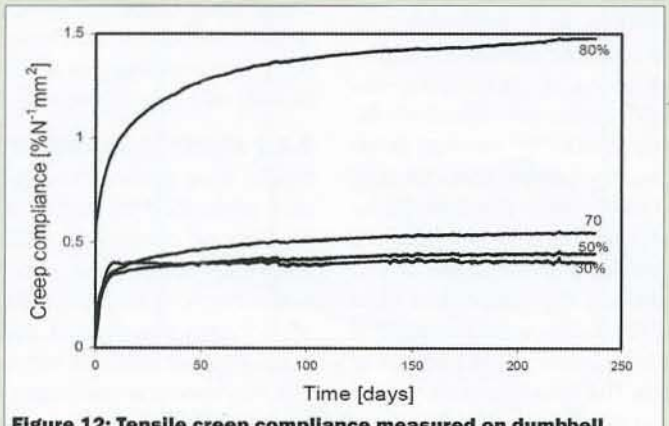

Figure 12: Tensile creep compliance measured on dumbbell SHCC specimens.

The initial rate-dependence is ascribed primarily to matrix cracking viscosity (Zhou 1992, Wu & Bažant 1993, van Zijl *et al.* 2001).

4 MODELLING OF SHCC TIME-DEPENDENT BEHAVIOUR

4.1 Computational framework

A continuum approach is followed. It is assumed that the tensile load-deformational behaviour measured over a practical gauge length on small specimens, for instance 80 mm on the dumbbell shown in *Figure 2*, is simply translated to stress-strain behaviour. *Figure 9* shows the assumed tensile material law, including a linear hardening and exponential softening tensile stress (σ_{ti}) - equivalent strain (κ_t) relation. The softening is controlled by fracture energy (g_{fti}). Note that the subscript i denotes the two material directions x and y respectively.

Anisotropy, which may be significant due to particular manufacturing processes, is considered. For instance, in extruded products dominant fibre orientation in the extrusion direction have been shown to cause flexural strength in the extrusion direction of roughly 2.5 times that in the orthogonal direction (Visser & van Zijl 2007). To account for such lower strength in the orthogonal direction, the same basic shaped stress-strain law as in *Figure 9* is used for tension in that direction, but with different values for first cracking stress (f_{ty}), ultimate tensile stress (f_{tuy}), strain at ultimate stress (κ_{tuy}), and fracture energy (g_{ty}), than those for the main material direction (f_{tx}, f_{tux}, κ_{tux} g_{tx}).

No test results for biaxial behaviour SHCC are available yet, with a test program for such behaviour currently in progress at the University of Stellenbosch. However, shear test results (Li *et al.* 1994, van Zijl 2007) indicate that SHCC shear resistance exceeds its uniaxial tensile resistance. Mechanisms include fibre confinement by compression orthogonal to the diagonal shear cracks, as well as steeper crack alignment to mobilise greater compressive resistance, enabled by retained tensile resistance beyond first cracking. These results imply non-trivial biaxial behaviour of SHCC, eg as shown by the dashed lines in *Figure 10*. For lack of sufficient characterising data, the solid line limit functions in *Figure 10* are assumed for the current computational framework.

Note that a plane stress state is considered and shown in *Figure 10* in terms of the two orthogonal normal stresses. This is appropriate for the thin-walled SHCC specimens used here.

Also shown in *Figure 10* are the limit functions for compression, which are also taken as simple straight lines in the zero shear stress (principal stress) plane. Similar expressions are used for the compressive stress-strain responses as for the tensile stress-strain model shown in *Figure 9*, with parameters f_{cx}, f_{cux}, κ_{cux}, g_{cx} and f_{cy}, f_{cuy}, κ_{cux}, g_{cy} respectively.

This is used for simplicity, but improved resemblance with the measured compressive responses - for example those in *Figure 4* - can easily be obtained by defining alternative hardening-softening curves, for instance parabolic hardening and linear softening.

4.2 Constitutive model for SHCC

In a plane stress setting with stress and strain vectors

$$\sigma^T = \left\lfloor \sigma_x \sigma_y \tau \right\rfloor, \varepsilon^T = \left\lfloor \varepsilon_x \varepsilon_y \gamma \right\rfloor \quad (1)$$

the material law can be expressed as follows

$$\dot{\sigma} = D^{ve}\dot{\varepsilon}^{ve} + \dot{\Sigma} = D^{ve}\left(\dot{\varepsilon} - \dot{\varepsilon}^{p} - \dot{\varepsilon}^{o}\right) + \dot{\Sigma} \quad (2)$$

where $\mathbf{D}^{ve}$ is an equivalent time-dependent stiffness modulus, ε^{ve}, ε^{p} and ε^{o} are the visco-elastic, plastic and initial strain vector respectively and Σ is a viscous stress vector accounting for the history. Full detail of the computational treatment is given by van Zijl *et al.* (2001). There it is shown that the visco-elastic stiffness is computed from the spring stiffnesses (E_i) and dashpot viscosities (η_i) of the elements in the Maxwell chain shown in *Figure 11*. The stress history term accumulates the stresses in each chain element at the end of the previous time step. Linear time integration is used to integrate eq. (2).

To incorporate the various sources of time dependence, the limit functions and their evolutions according to the hardening-softening shown in *Figure 9* are enhanced by consideration of bulk visco-elasticity through the Maxwell-chain, as well as cracking viscosity (η_{cr}), as schematised in *Figure 11*. Note that the latter is activated only in tension.

The limit stresses are treated in multi-surface plasticity fashion, whereby the plastic strain increment is expressed as follows:

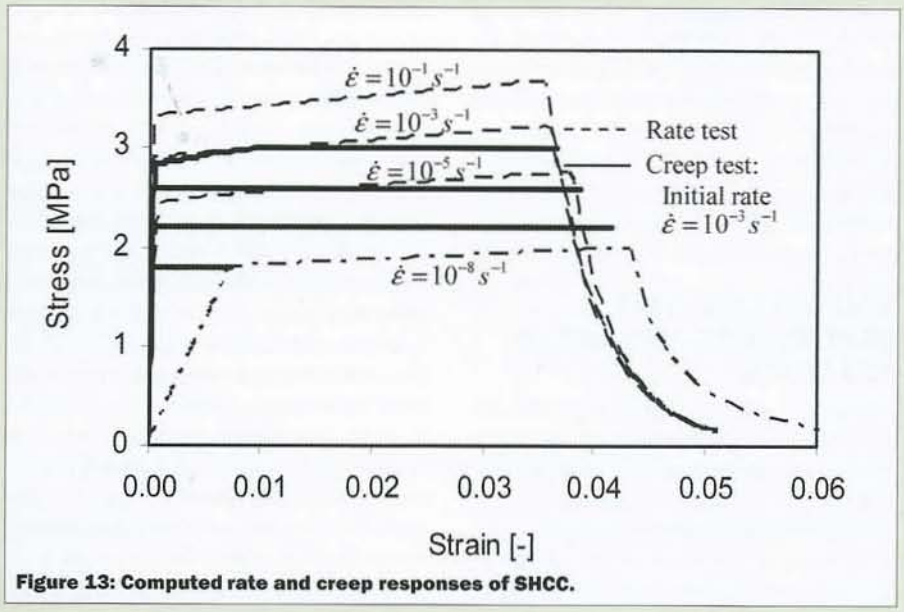

Figure 13: Computed rate and creep responses of SHCC.

$$\Delta\varepsilon^{p} = \Delta\lambda \frac{\partial f}{\partial \sigma} \quad (3)$$

with λ the amount of plastic flow/crack strain and f the flow function. For tension, the anisotropic Rankine yield function is chosen (represented by the solid line in *Figure 10*), which is a maximum principal stress failure criterion, formulated as

$$f_t = \frac{(\sigma_x - \sigma_{tx}) + (\sigma_y - \sigma_{ty})}{2} + \sqrt{\left(\frac{(\sigma_x - \sigma_{tx}) + (\sigma_y - \sigma_{ty})}{2}\right)^2 + \alpha_t \tau^2} \quad (4)$$

The current admissible stresses in the material x, y directions are denoted by σ_{tx} and σ_{ty} respectively.

Simple expressions for the tensile resistance are given in *Figure 9*. As stated in the previous section, separate expressions are used in the orthogonal directions, with separate sets of model parameters. The hardening-softening is governed by equivalent tensile strain K_t, with an appropriate measure for SHCC considered to be the maximum principal plastic strain given by

$$\dot{\kappa}_t = \dot{\varepsilon}_1^{p} = \frac{\dot{\varepsilon}_x^{p} + \dot{\varepsilon}_y^{p}}{2} + \sqrt{\left(\frac{\dot{\varepsilon}_x^{p} - \dot{\varepsilon}_y^{p}}{2}\right)^2 + \left(\frac{\dot{\gamma}}{2}\right)^2} \quad (5)$$

The equivalent strain increment can be shown to be directly related to the plastic flow increment ($\Delta K_t = \Delta\lambda_t$) insert symbols. The parameter α_t controls the shear contribution to tensile failure.
In compression, the limit function is

$$f_c = -\frac{(\sigma_x - \sigma_{cx}) + (\sigma_y - \sigma_{cy})}{2} + \sqrt{\left(\frac{(\sigma_x - \sigma_{cx}) + (\sigma_y - \sigma_{cy})}{2}\right)^2 + \alpha_c \tau^2} \quad (6)$$

The equivalent compressive strain is

$$\dot{K}_c = \dot{\varepsilon}\frac{p}{2} = \frac{\dot{\varepsilon}\frac{p}{x} + \dot{\varepsilon}\frac{p}{y}}{2} + \sqrt{\left(\frac{\dot{\varepsilon}\frac{p}{x} - \dot{\varepsilon}\frac{p}{y}}{2}\right)^2 + \left(\frac{\dot{\gamma}}{2}\right)^2} \quad (7)$$

As for tension, it can be shown that the $\Delta K_c = \Delta\lambda_c$.

The intersection between the two limit surfaces is treated in a consistent way, as proposed by Koiter (1953).

$$\Delta\varepsilon^{p} = \Delta\lambda_t \frac{\partial f_t}{\partial \sigma} + \Delta\lambda_c \frac{\partial f_c}{\partial \sigma} \quad (8)$$

In tension, a cracking rate-dependence is introduced following Wu & Bažant (1993) and van Zijl *et al.* (2001) as follows:

$$\Delta w = \Delta w_r \sinh\left[\frac{\sigma - \sigma_t(w)}{c_1\left[\sigma_t(w) + c_2 f_t\right]}\right] \quad (9)$$

where w_r is a constant, reference crack opening rate.

The crack width w, which is assumed to be spread uniformly across the fracture process zone of width l_b, can be related to the equivalent strain as follows:

$$K_t = w / l_b \quad (10)$$

With eqs. (9, 10) the tensile strength equations (*Figure 9*) can be rewritten as

$$\sigma_{ti} = \left(f_{ti} + \frac{f_{tui} - f_{ti}}{K_{tui}} K_t\right) \Big/ \left[1 + c_1 \sinh^{-1}\left(\frac{\dot{K}_t}{\dot{K}_r}\right)\right] + c_1 c_2 f_{tui} \sinh^{-1}\left(\frac{\dot{K}_t}{\dot{K}_r}\right) \quad \forall \quad K_t \le K_{tui} \quad (11)$$

$$\sigma_{ti} = f_{tui\exp}\left(\frac{-f_{tui}}{G_{fi}/l_b}(K_t - K_{tui})\right) \Big/ \left[1 + c_1 \sinh^{-1}\left(\frac{\dot{K}_t}{\dot{K}_r}\right)\right] + c_1 c_2 f_{tui} \sinh^{-1}\left(\frac{\dot{K}_t}{\dot{K}r}\right) \quad \forall \quad K_t > K_{tui} \quad (12)$$

where the index i refers to the materials axes. The coefficient c_2 is a small offset value to prevent singularity of eq. (9). The reference strain $\dot{K}_r$ rate is directly related to w_r cf. eq. (10).

It should be a sufficiently low cracking rate at which the cracking strengths are rate-independent. In the current model, the rate terms represent all physical processes causing rate dependence, including both cracking viscosity and fibre pull-out rate-dependence. The constitutive model has been implemented as a user material in DIANA (2008).

5 MODELLING RATE DEPENDENCE AND CREEP FRACTURE

The ability of the model to represent observed SHCC rate-dependence and creep is demonstrated in this section. The simple case of uniaxial tension is considered here, representing the case for which the results are shown in *Figure 5*. The model parameters were taken as average values of the following test results:

(i) Monotonic, uniaxial tensile tests at low rates on dumbbell specimens to obtain the quasi-static tensile strength and hardening-softening parameters.

Note however that the lowest physical test load rate of $\dot{\varepsilon} = 10^{-5}\, s^{-1}$ was used. To incorporate lower tensile resistance at an even lower rate, the reduced values f_{tx} = 1.8 MPa, f_{tux} = 2.0 MPa, K_{tux} = 0.035 and g_{tx} = 0.01 N.mm^{-2} were chosen by inverse analysis to represent the case for $\dot{\varepsilon} = \dot{K}_r = 10^{-8}\, s^{-1}$.

(ii) Tensile creep tests on dumbbell specimens to compute spring stiffness and dashpost viscosities in the linear visco-elastic range, ie up to 50% of peak load – *Figure 12* shows that tensile creep loads beyond 50% lead to nonlinear creep. Note that shrinkage has been measured on separate specimens and has been compensated for.

(iii) Rate-dependent tensile tests on dumbbell specimens, from which the cracking rate model (eqs. 11, 12) parameters were computed by inverse analysis:

$$c_1 = 0.05, c_2 = 0.001 \; and \; \dot{K}_r = 10^{-8}\, s^{-1}$$

The finite element model results computed with the constitutive model are presented in *Figure 13*. The numerical results of rate-dependent tensile tests are shown in dashed lines, with tensile strain rates coinciding with those in the physical experiments (*Figure 5*).

Also shown in the figure are numerical results of tensile creep analyses at various levels of sustained load (1.8, 2.4, 2.8 and 3.2 MPa). The results indicate that the creep limit is reached for tensile creep at a sustained load level below a certain threshold, in this case 2 MPa. Delayed fracture of the specimen does not occur at loads below this level. Beyond this level, creep fracture occurs after significant creep deformation. This is in agreement with the experimental results for the case of 80% sustained load in *Figure 5*, except that the physical specimens have not yet fractured. Nevertheless, delayed fracture is expected, based on reported creep fracture at high sustained tensile load (Jun & Mechtcherine 2007) and observed in tensile creep tests on notched SHCC specimens (Boshoff *et al.* 2008).

Note further that the computed responses to the rate-dependent, monotonic tests form an envelope of deformability for the creep specimens, beyond which creep fracture occurs.

The numerical results shown in *Figure 13* are in reasonable agreement with the measured responses in *Figure 5*. Note however, that no attempt was made to incorporate a strain-dependent rate term to simulate the different mechanisms of rate-dependence described in section 3.2.3. By such distinction, improved agreement with experimental results may be obtained.

6 CONCLUSIONS

This paper proposes a constitutive model for SHCC. Mechanisms of tensile creep and rate-dependence have been identified from recent experimental results. Rate-dependence of the cement-based matrix is considered to dominate in the low deformation range after first cracking, while rate-dependent fibre pull-out governs the response at large deformations.

The constitutive model incorporates anisotropy in terms of different strengths and strain-hardening-softening curves for orthogonal material directions, for both tension and compression. The framework of multi-surface continuum plasticity is used and extended to incorporate visco-elasticity for the bulk creep and cracking rate-dependence.

The model requires further characterisation for biaxial loading. For lack of such data, simple Rankine-type limit functions have been suggested and elaborated here. Current research activities include biaxial testing of SHCC to investigate whether the linear functions are appropriate.

The model has been implemented as a user material in a commercial finite element programme and used in finite element analyses to demonstrate its ability to capture the phenomena of creep, creep fracture and rate-dependence with reasonable accuracy.

However, the model does not distinguish between the identified different physical mechanisms of rate-dependence, acting at different levels of deformation in SHCC. This is a continued research focus.

ACKNOWLEDGEMENTS

This research has been performed under the THRIP project SAPERCS. The Department of Trade and Industry and the industry partners of this project, namely Infraset, the Cement and Concrete Institute, Grinaker-LTA, Africon, BKS, Element Consulting Engineers are gratefully acknowledged.

Ingredient materials were generously donated by PPC (cement), Chryso South Africa (chemical additives) and Kuraray Japan (PVA fibres).

The research results of Heinrich Stander (MScEng, 2007), Christo Visser (MScEng, 2007) and Dr Billy Boshoff (PhD, 2007) at Stellenbosch University have been invaluable in this work.

REFERENCES

1. Bažant, Z P, and Najjar, L J 1971. Drying of Concrete as a Non-Linear Diffusion Problem, Cement and Concrete Research 1, pp. 461-473.
2. Boshoff, W P 2007. Time-dependant behaviour of ECC, PhD dissertation, Stellenbosch University, South Africa.
3. Boshoff, W P Adendorff, C and GPAG van Zijl, 2008. Creep of Cracked Strain-Hardening Cement-based Composites, CONCREEP8, Sept 2008, Tokyo.
4. Boshoff W P and van Zijl, G P A G 2007. A computational model for strain-hardening fibre-reinforced cement-based composites. J SAICE, 49(2) 24-31.
5. DIANA v 9.3, 2008. DIANA Users Manual, TNO DIANA BV, Delft, The Netherlands.
6. Jun, P and Mechtcherine, V. 2007. Behaviour of SHCC under repeated tensile loading, RILEM PRO 53: HPFRCC5, Mainz, Germany pp. 97-104.
7. Kabele, P 2002. Equivalent continuum model of multiple cracking, Engng. Fracture Mechanics, 9(1/2), pp. 75-90.
8. Koiter, W T 1953. Stress-strain relations, uniqueness and variational theorems for elastic-plastic materials with singular yield surface, Q. Appl. Math. 11(3), pp. 350-354.
9. Lepech, M and Li, V. C. 2005. Water

REFERENCES continued

Permeability of Cracked Cementitious Composites, Proceedings of ICF11, Turin, Italy, Mar. 2005, pp. 113-130.

10. Li, V C Mishra, D K Wu, H.C. 1995. Matrix design for pseudo strain-hardening FRCC, Materials and Structures, 28, pp. 586-595.
11. Li, V C, Mishra, D K, Naaman, A E, Wigh, J K, LaFave, J M, Wu, H C and Inada, Y, 1994. On the shear behavior of engineered cementitious composites, Journal of Advanced Cement Based Materials 1 (3), pp. 142–149.
12. Neithalath, N 2006. Analysis of Moisture Transport in Mortars and Concrete using Sorption-Diffusion Approach, ACI Materials J. 103(3), 209-217.
13. Rapoport, J, Aldea C, Shah, S P, Ankenman, B and Karr, A F 2001. Permeability of Cracked Steel Fibre-Reinforced Concrete. Technical Report Number 115, January, 2001, National Institute of Statistical Sciences.
14. Rüsch, H 1960. Researches toward a general flexural theory for structural concrete, ACI J. 57(1), pp. 1-28.
15. Sahmaran, M, M Li, and V C Li 2007. Transport Properties of Engineered Cementitious Composites Under Chloride Exposure, ACI Materials J. 104(6), 604-611.
16. Shang Q J and van Zijl G P A G. (2007). Characterising the shear behaviour of SHCC. J SAICE, 49(2) 16-23.
17. Van Zijl, G P A G 2005. The role of aggregate in high performance fibre-reinforced cement-based composites. Concrete Beton, Nr 110, September 2005, pp. 7-13.
18. Van Zijl, G P A G 2007. Improved mechanical performance: Shear behaviour of strain hardening cement-based composites (SHCC). Cem. and Concr. Res., 37(8), pp. 1241-1247.
19. Van Zijl, G P A G. 2008. Durability of strain-hardening cement composites (SHCC) – an overview, CDROM Proc. ICCRRR, Nov 2008, Cape Town.
20. Van Zijl, G P A G, de Borst, R and Rots, J G (2001). The role of crack rate dependence in the long-term behaviour of cementitious materials. Int. J. Solids and Structures, 38(30-31), pp. 5063-5079.
21. Visser, C R and van Zijl, G P A G 2007. Mechanical characterisation of extruded SHCC, RILEM PRO 53: HPFRCC5, Mainz, Germany pp. 165-173.
22. Wang, K, Jansen, D C, Shah, S, and Karr, A F 1997. Permeability study of cracked concrete, Cement and Concrete Research, 27(3) 381-393, 1997.
23. Weimann, M B and Li, V C 2003. Hygral Behavior of Engineered Cementitious Composites (ECC), International Journal for Restoration of Buildings and Monuments 9(5), 513–534.
24. Wu, Z S and Bažant, Z P 1993. Finite element modelling of rate effect in concrete fracture with influence of creep, Creep and Shrinkage of Concrete (eds. Z P Bažant and I.Carol), E.&F.N.Spon, London, pp. 427-432.
25. Zhou, F P 1992, "Time-dependent Crack Growth and Fracture in Concrete," PhD thesis, University of Lund, Sweden.